1-1-2016

Micro/Nano-Structural Examination and Fission Product Identification in Neutron Irradiated AGR-1 TRISO Fuel

I. J. van Rooyen
Idaho National Laboratory

T. M. Lillo
Idaho National Laboratory

H. M. Wen
Idaho National Laboratory

C. M. Hill
Idaho National Laboratory

T. G. Holesinger
Los Alamos National Laboratory

See next page for additional authors

MICRO/NANO-STRUCTURAL EXAMINATION AND FISSION PRODUCT IDENTIFICATION IN NEUTRON IRRADIATED AGR-1 TRISO FUEL

I.J. van Rooyen,[a] T.M. Lillo,[b] H.M. Wen,[a,c] C.M. Hill,[d] T.G. Holesinger,[e] Y.Q. Wu,[f,g] and J.A. Aguiar[a]

[a] *Fuel Design and Development Department, Idaho National Laboratory, Idaho Falls, ID 83415-6188, USA*
Email: isabella.vanrooyen@inl.gov
[b] *Materials Science and Engineering Department, Idaho National Laboratory, Idaho Falls, ID 83415-2211, USA*
[c] *Department of Physics, Nuclear and Electrical Engineering, Idaho State University, Idaho Falls, ID 83402, USA*
[d] *Experiment Analysis Department, Idaho National Laboratory, Idaho Falls, ID 83415-6188, USA*
[e] *Science and Technology Division, Los Alamos National Laboratory, Los Alamos, USA*
[f] *Micron School of Materials Science and Engineering, Boise State University, Boise, ID 83725, USA*
[g] *Center for Advanced Energy Studies, Idaho Falls, ID 83401, USA*

Advanced electron microscopic and micro-analysis techniques were developed and applied to study irradiation effects and fission-product behavior in selected low-enriched uranium-oxide/uranium-carbide tristructural-isotropic (TRISO)-coated particles from fuel compacts in four capsules irradiated to burnups of 11.2 to 19.6% fissions per initial metal atom (FIMA) consisting of Baseline, Variant 1, and Variant 3 fuel types. Trend analysis shows precipitates were mostly random in their distribution along the perimeter of the inner pyrolytic carbon-silicon carbide (IPyC-SiC) interlayer with only weak association with kernel protrusion and buffer fractures. Pd is dominantly found in most precipitates in both intra and intergranular locations. Nano-sized Ag is predominantly found in grain boundaries and triple points with only two findings of Ag inside a SiC grain in two different compacts (Baseline and Variant 3 fueled compacts). Generally, more element combinations exist for precipitates from particles with relatively low Ag retention compared to particles with relatively high Ag-retention irrespective of fuel type. This study shows the presence of Cs in particles from all compacts evaluated. From this work, no single fission product mechanism hypothesis can be reported. The complexity of mechanisms is further highlighted by the multiple variations of elemental combinations found in the more than 700 fission product precipitates examined. It seems that movement of Ag is not assisted by a specific element in all cases. Therefore, it is not necessarily true that a chemical-assisted transport mechanism is dominant. The presence of Ag predominantly on grain boundaries suggests that a grain boundary transport mechanism may be prominent. Studies to determine the effect of neutron damage are recommended for future work.

I. INTRODUCTION

A series of up to seven irradiation experiments are planned for the Advanced Gas Reactor (AGR)-fuel development and qualification program,[1] with irradiation completed for the first experiment (AGR-1) in November 2009 for an effective 620 full power days. The AGR-1 nuclear fuel particles were fabricated at Oak Ridge National Laboratory (ORNL) using 350-µm-diameter mixed uranium-oxide/uranium-carbide (UCO) kernels at 19.74 wt.% ^{235}U enrichment, produced by BWX Technologies, Inc. Nuclear Operations Group. These kernels were subsequently coated via fluidized-bed chemical vapor deposition (FBCVD) with a porous buffer layer ≈100 µm, a dense inner pyrolytic carbon (IPyC) layer ≈40 µm, a silicon carbide (SiC) structural containment layer ≈35µm, and a dense outer pyrolytic carbon (OPyC) layer ≈40 µm to form the Baseline tristructural-isotropic (TRISO) particle. These layers were deposited in sequence, without removing particles from the coating chamber, with an argon gas purge between steps. Approximately 4100 particles were then over-coated with natural and synthetic graphite in a thermosetting resin and pressed into cylindrical compacts.[2,3,4,5]

The AGR-1 experiment contained four types (called Baseline and Variants 1–3) of TRISO-coated particles, fabricated with varying conditions, although in this paper the microstructural examination observations from selected particles of only three fuel types namely, Baseline, Variant 1, and Variant 3 are discussed to establish potential trends in fission product identification, distribution, and SiC layer integrity. Particles were selected for this study to allow comparison of the fission-product distribution with particle ^{110m}Ag retention, fuel type, and compact irradiation level.

Earlier microstructural examination on neutron irradiated TRISO coated particles to study fission product distribution, and the associated grain boundary characteristics, included mainly: scanning electron microscopy (SEM), electron back scatter diffraction (EBSD) and electron probe micro-analysis (EPMA).[6,7,8,9,10,11,12] Although these techniques provide valuable macro and micro level information, they could not resolve the nano-sized fission product locations through the SiC layers. Therefore, other techniques were explored as discussed by van Rooyen et al in Refs. 10 and 13.

This paper provides an overview of the electron microscopy and micro analytical activities performed as part of the AGR-1 PIE at INL. Selected results obtained from SEM, atom-probe tomography (APT), transmission electron microscopy (TEM), scanning transmission electron microscopy (STEM), and high-resolution transmission electron microscopy (HRTEM) examinations. The electron probe micro-analysis (EPMA) results on fission product distribution patterns and precession electron diffraction (PED) for grain boundary character distributions are discussed in separate conference papers by Lillo et al[14] and Wright et al.[15]

II. METHODS

II.A. Fuel type and Selected Fission Products Release Inventory of AGR-1 Experiment

Fabrication parameter conditions differentiating the different fuel types are shown in Table I, with the objective of these changes listed. The AGR-1 experiment consisted of six capsules, each filled with 12 fuel compacts of similar fuel type, stacked in a 3 × 4 array, for a total of 72 compacts. (details of the experiments are discussed in Refs. 5 and 16).

Post-irradiation examination (PIE) was conducted to ascertain fission-product release from fuel compacts in addition to the evaluation of burnup levels. The radio-nuclides of highest concentration found in capsule components outside of the fuel compacts include: ^{110m}Ag, ^{134}Cs, ^{137}Cs, ^{154}Eu, and ^{90}Sr. Fractional inventory per capsule, measured vs. calculated, of selective isotopes is provided in Table II. The highest fractional release measured outside of the compacts is associated with ^{110m}Ag, ranging from 1.2 (from Capsule 3) to 38% (from Capsule 6) of calculated inventory. Fractional inventories within individual compacts varied widely within a particular capsule (see Ref. 17). ^{134}Cs-retention values were excellent for Capsules 1–4, and gamma analysis of the compact holders led to the isolation of a single coated particle with a failed SiC layer within a specific compact in Capsule 6 and three coated particles with failed SiC layers in Capsule 5 (see Ref. 18). Amongst approximately 300,000 AGR-1 TRISO fuel particles tested, in no case was there a complete failure of all three outer coatings. Capsules 1 and 4, both housing Variant-3 fuel type compacts, have the lowest fractional inventory of ^{154}Eu and the highest fractional inventory of ^{90}Sr found in the capsule components.[16]

TABLE I. Variation in baseline process parameter for four TRISO particle types (adapted from Ref. 4).

Fuel Type	IPyC temp. (°C)	IPyC coating gas fraction	SiC temp. (°C)
Baseline	1265	0.30	1500
Fabricated to closely match historically proven German fuel containing UO_2 particles.			
Variant 1	1290	0.30	1500
Enhanced irradiation stability of the pyrocarbon (PyC), although permeability expected to increase and, consequently, uranium dispersion (IPyC layer less dense than that in baseline fuel) by changing IPyC deposition temperature.			
Variant 3[a]	1265	0.30	1425
Reduce the potential for SiC-layer defects resulting from uranium dispersion and provide a change in polycrystalline microstructure that may be less permeable to metallic fission			

[a] Variant 3 SiC was deposited using 50:50 mix of argon:hydrogen (Ar:H) for the fluidization gas.

TABLE II. Total fractional inventory of selected fission products found in the AGR-1 capsule components (adapted from Ref. 16).

Capsule	^{110m}Ag	^{134}Cs	^{154}Eu	^{90}Sr
6	3.8E-01	1.33 E-05	4.75E-04	3.15E-06
5	2.3E-01	1.22E-05	1.43E-04	7.14E-06
4	1.3E-01	<2.4E-06	<1.4E-04	9.75E-06
3	1.2E-02	<2.5E-06	4.46E-04	2.20E-06
2	5.5E-02	<1.2E-06	1.65E-04	8.42E-07
1	3.6E-01	<2.8E-06	1.3E-04	2.48E-05

II.B. Particle Selection and Irradiation Conditions

Microstructural work in early 2012 focused on the analysis of the Baseline fuel type, specifically, on particles from Compact 6-3-2 (see Ref. 8). This earlier work was exploratory to establish knowledge on fission-product location and features to refine the SEM analysis techniques necessary to achieve the microstructural characterization objectives and to identify specific areas or features of interest.[8] A key component of AGR-1 PIE was to examine various particles based upon their observed ^{110m}Ag retention, determined by gamma-counting data, in an attempt to correlate Ag-retention behavior with specific SiC layer characteristics, irradiation effects, and fabrication features. For this work, an expanded data set from TRISO-coated particles from compacts 6-3-2, 5-3-1, 5-2-3, 4-1-1,

1-3-1, and 4-3-3 are tabulated and compared. Generally, particles from each compact were selected to represent a low- and high-Ag-retention particle. Estimated Ag-retention values are determined by comparing the measured ^{110m}Ag activity in each particle to the predicted inventory from physics calculations. Values in excess of 100% are possible if Ag retention in the particle was high, and the calculated inventory was biased low (details of the selection criteria are described by Demkowicz et al [2015] Ref. 19). Note that retention values are relatively high and low for the specific particles in each compact for which Ag was measured.

For these studies, coated particles from one Baseline fuel type compact, two Variant 1 fuel type compacts and three Variant 3 fuel compacts were chosen. The irradiation conditions for the selected AGR-1 compacts are shown in Table III.

TABLE III. Irradiation conditions for AGR-1 experiment selected compacts (adapted from Demkowicz et al. [2015] Ref. 19).

Compact	Fuel Type	Burnup (%FIMA)	Fast Neutron Fluence*	Time-Average Volume Average Temp. (°C)	Time-Average Peak Temp. (°C)
6-3-2	Baseline	11.4	2.55	1070	1144
5-3-1	Variant 1	16.7	3.60	1040	1122
5-2-3	Variant 1	17.4	3.77	1059	1141
1-3-1	Variant 3	15.3	3.22	1092	1166
4-1-1	Variant 3	19.4	4.13	1072	1182
4-3-3	Variant 3	18.6	4.16	1094	1179

(*10^{25} n/m^2 E > 0.18 MeV)

Unfortunately, in the case of Compact 6-3-2 (the Baseline fuel type compact), the low-retention particle (AGR1-632-030) was over-polished, and important SiC-IPyC interface features were lost. Therefore, only the high-retention particles (AGR1-632-034 and AGR1-632-035) were examined. Particles from the two Variant 1 compacts include: (a) a high- and low- ^{110m}Ag retention particle for comparative microstructural analysis and (b) one particle from Compact 5-2-3 which was identified after an interesting IPyC fracture was observed during three-dimensional (3-D) tomography studies conducted by ORNL.[18] Therefore, particle selection for advanced characterization does not comply with the normal high- and low-Ag selection criteria.

The three Variant 3 compacts include: (a) Compact 4-3-3, which was safety tested at 1600°C (see Ref. 20) to examine the effect that high-temperature, post-irradiation heating may have on microstructure in correspondence with ^{110m}Ag retention, (b) Compact 1-3-1 from which a high- and low- ^{110m}Ag retention particles were chosen, and (c) a particle with relatively high- ^{110m}Ag retention (90% retention) from Compact 4-1-1. Particle (c) was submitted for atomic resolution examination to develop a detailed understanding of the structure and crystallography associated with fission products measuring less than 40 nm and as small as 2 nm. Images were recorded in HRTEM and HRSTEM modes.

II.C. Methods and Techniques

The methods employed to study the micro-/nano-structural features in focused ion beam (FIB)-prepared lamellae of neutron-irradiated TRISO-coated particles are described in earlier papers.[21,22,23] Table IV indicates (by an X) the electron microscopy and micro-analytical techniques used to study the specific coated particles described in this paper. The specific particle number scheme is described by Demkowicz et al. (2015) (see Ref. 19), and provides information on the compact number which embodies the original location in the test train and a uniquely identified particle within the compact.

TABLE IV. Electron microscopic and micro-analytical analysis matrix for AGR-1 experiment selected compacts.

SEM	STEM	EPMA	PED	APT	HRTEM
Compact 6-3-2 (Baseline)					
Particle AGR1-632-030 (Low Ag (21%) retention)					
X	—	—	—	—	—
Particle AGR1-632-034 (High Ag (65 %) retention)					
X	X	—	—	X	—
Particle AGR1-632-035 (High (79%) Ag retention					
X	X	—	X	X	—
Compact 5-3-1 (Variant 1)					
AGR1-531-038 (Low (< 19%) Ag retention) AGR1-531-031 (High (105%) Ag retention)					
X	X	—	X	—	—
Compact 5-2-3 (Variant 1)					
Particle AGR-523-SP01					
—	X	—	X	—	—
Compact 1-3-1 (Variant 3)					
Particle AGR1-131-099 (Low (<6 %) Ag retention) Particle AGR1-131-066 (High (39%) Ag retention)					
X	X	—	X	—	X
Compact 4-1-1 (Variant 3)					
Particle AGR1-411-030 (High Ag (90%) retention)					
X	—	—	—	—	X
Compact 4-3-3 (Variant 3; 1600°C safety tested)					
Particle AGR1-433-003 (Low (< 22%) Ag retention Particle AGR1-433-007 (High (100%) Ag retention					
—	—	X	—	—	—
Particle AGR1-433-001 (Low (66%) Ag retention) Particle AGR1-433-004 (High (99%) Ag retention)					
X	X	—	X	—	X

III. RESULTS

Due to the limitations and gaps identified during the initial SEM analysis of particles from Compact 6-3-2, more advanced electron microscopy and micro-analysis techniques were identified and explored. There are some knowledge gaps that required further exploration. The results reported in this paper aim to address these gaps while mentioning any remaining shortfalls as follows: (a) accurate quantification of elemental composition, (b) accurate distribution of elements in a specific precipitate, (c) phases of the fission-product precipitates, (d) transport mechanisms throughout the intact layers (specifically for Ag and Pd), and (e) fission-product crystallographic properties and grain-boundary characteristics.

III.A. Fission-product Location Maps Using SEM Montages

SEM analysis initially focused on the location, rather than chemical composition, of fission products because quantification was problematic due to the relatively small size of the precipitates, X-ray-energy overlaps of constituents in the precipitate clusters, and the use of both standardless energy dispersive X-ray spectroscopy (EDS) and wavelength dispersive X-ray spectroscopy (WDS) methods. The presence of U and Pd made detection of low concentrations of Ag particularly challenging because all of the major Ag X-ray peaks with energies below ≈20 keV have energies that are similar to those from high-relative-intensity peaks from U or Pd, thus, making it impossible to qualitatively detect Ag using an energy dispersive X-ray (EDX) detector measuring within this energy range.[23] (Efforts to detect Ag in the precipitates continued as part of the AGR-1 PIE in microscopes where silicon-drift EDX detectors with a normal 0–40 keV range were available).

A detailed fission product distribution montage method was developed to determine possible relationships between fission-product-cluster location and other microstructural features like kernel protrusion, fractures in the IPyC, or breached buffer layers.[23,24] Figure 1(a) shows, as an example, one of the montages prepared for particle AGR1-131-066 with the particle cross section image in Figure 1(b). Trend analysis shows precipitates were randomly distributed along the perimeter of the IPyC-SiC interlayer with a slight association with kernel protrusion and buffer fractures. A slightly higher concentration of fission product clusters were found in the region where the kernel is closer to the IPyC-SiC interlayer. As it was not possible to distinguish sufficiently between Ag, U, and Pd, no specific observation could be made towards the distribution of Ag-containing precipitates while studying these montages. Therefore, it was concluded that these montage analyses showed only weak relations with the kernel morphology, and it is considered that the resolution of the imaging and corresponding developed method may not be sufficient to identify trends and relations to the features and fission products in the different layers. More fission-product clusters were identified in the SiC layer in particles from Variant 3 compact 1-3-1 compared with Variant 1 compact 5-3-1.

The SiC-IPyC interlayer thickness (a representative example in Figure 1[c]) was considered a potential differentiating parameter to determine fission-product retention—specifically Ag retention. (A discussion on interlayer thickness measurement and montages are described in van Rooyen et al [2014] [see Ref. 23]). Even though there was a particle-to-particle interlayer thickness variation (interlayer thicknesses typically from 2–3 µm); it was found that Variant 3 particles exhibited a thicker interlayer. Although the higher Ag-retaining particle, AGR1-131-066, had a thicker interlayer than the lower Ag-retaining particle, AGR1-131-099. The same trend was not observed for the particles from Compact 5-3-1, a Variant 1 fuel type.

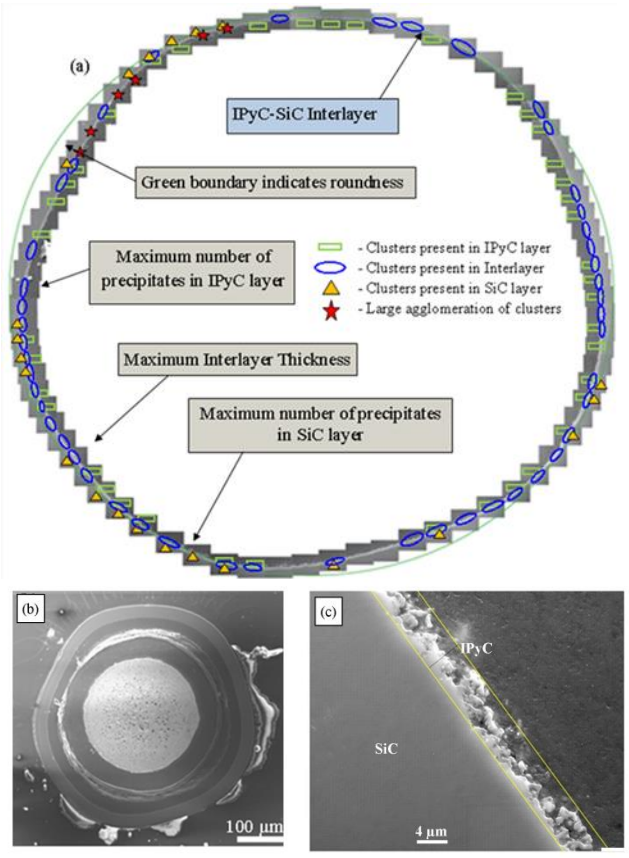

Fig. 1. (a) SEM image montage depicting the distribution of precipitates in Particle AGR1-131-066, (b) SEM image of the particle cross-section at mid-plane, and (c) representative SEM image SiC-IPyC interlayer thickness marked between the yellow lines.

EPMA was further explored as a quantitative tool to determine effects of kernel morphologies and other features on fission-product distribution and Ag retention trends (see HTR2016 paper 18570 [Ref. 15]).

III.B. Identification of Ag in Grain Boundaries and Triple Points Using STEM/TEM/HRTEM based EDS Analysis

One of the first breakthroughs from advanced microscopic and micro-analysis was the identification of nano-sized Ag precipitates in grain boundaries and triple points in particle AGR1-632-035 in the SiC layer at the SiC-IPyC interface, as shown in Figure 2 (see Ref. 25).

Subsequent electron microscopy examination revealed similar nano-Ag precipitates in grain boundaries and triple points in most of the other particles studied from other compacts, fabricated from all variant fuel types. Ag was often found in concert with cadmium (Cd) and/or Pd, as identified during the earlier studies on particles from Compact 4-1-1 (see Refs. 10, 21, and 26) and Compact 1-3-1 (see Refs. 27 and 28). Figure 3(a) shows a typical example of Ag and Pd co-existence within the IPyC layer near the interface with SiC from particle AGR1-131-099.

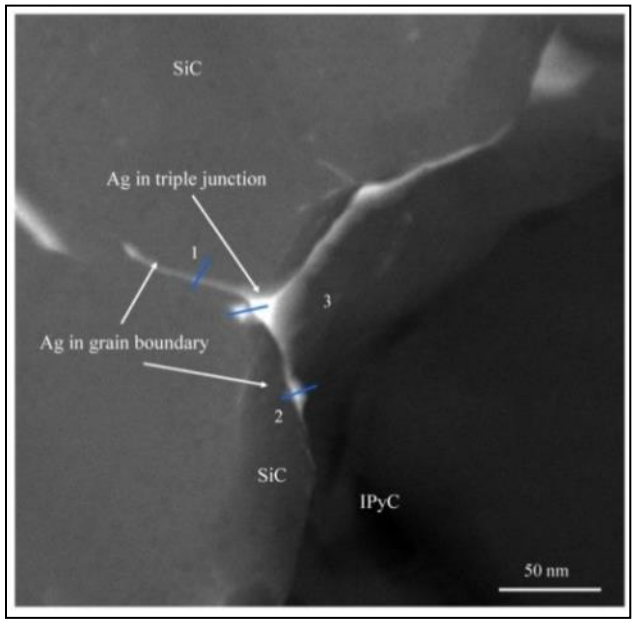

Fig. 2. Image showing the HAADF STEM image of Ag-containing grain boundaries and triple junction at the inner area of the SiC adjacent to the IPyC from particle AGR1-632-035 (see Ref. 25).

Additionally, an example of Ag found in a grain boundary close to the SiC-IPyC interface from particle AGR1-433-001 is shown in Figure 4. Figure 4(a) is a high angle annular dark field (HAADF) STEM image showing the significant distribution of fission product precipitates. A closer examination of the fission product precipitation along a specific grain boundary is found in Figure 4(b) and in Figure 4(c) outlined with a blue box. Figure 4(d) shows STEM EDS spectrum at the grain boundary precipitate and shows the presence of Pd and Ag.

The STEM EDS is qualitative or semi-quantitative in nature given the smaller sample volume of the precipitates buried within a SiC matrix. Consequently, quantification of the collected lower signal to background EDS was performed to identify elements that meet a 3:1 signal to background count threshold criterion and are quantified above 0.2 at.%, which is the specified limit of detection provided by our detector manufacturer, EDAX.

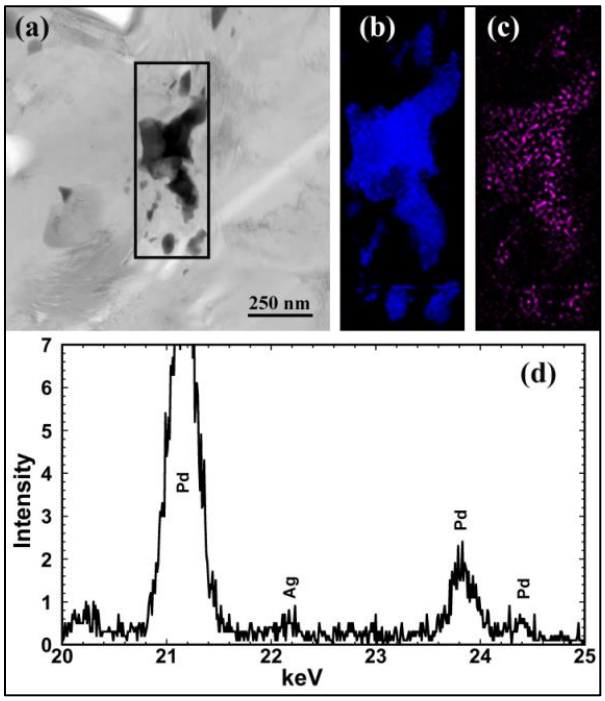

Fig. 3. STEM bright-field image (a) with corresponding EDS spectral images for (b) Pd and (c) Ag, showing their co-existence in a precipitate from AGR1-131-099. The maximum concentration of Pd and Ag at any one point from semi-quantitative analysis of the spectral data was 38.5 and 4.4 at.%, respectively. An average spectra derived from fifteen random spectra extracted from the area highlighted as containing Ag in the spectral map is shown in (d).

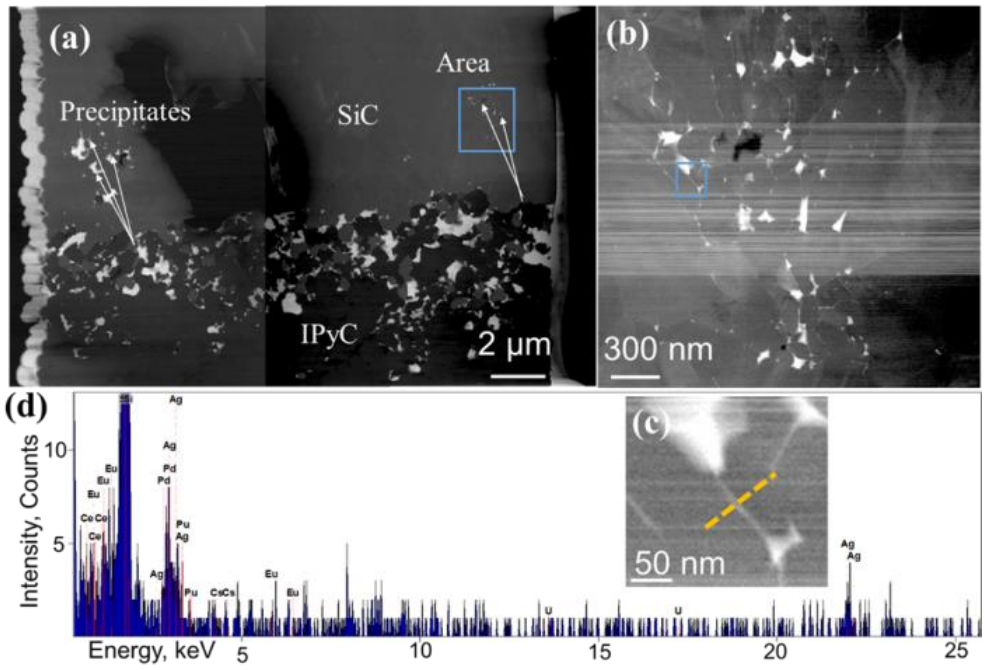

Fig. 4. (a) HAADF STEM image taken near the SiC-IPyC interface from particle AGR1-433-001, shows the significant distribution of fission product precipitates; (b) larger magnifications of image marked with a blue box in (a) which shows in (c) fission product precipitation along a specific grain boundary outlined with a blue box, (d) STEM EDS spectrum identifies Pd and Ag, amongst Eu, Ce, Cs and Pu. Ag measures less than 1 at.%, at this specific grain boundary.

III.C. Finding of Ag Intragranularly in SiC

During the advanced microscopy studies of AGR-1 coated particles, two findings of Ag inside a SiC grain (Figures 5 (b & d) and 6) were detected. This is in contrast with the predominant finding of Ag at SiC grain boundaries and triple points of AGR-1 coated particles. Figure 6 shows an Ag-Pd-Cd precipitate at a stacking fault (red arrows in Figure 6[c]) inside a SiC grain. The continuous lattice fringes (Figures 6[d] and [e]) across the stacking faults indicate absence of a grain boundary or a twin boundary and confirm the presence of stacking faults.

Therefore, it can be determined the Ag-Pd-Cd precipitate is located at a stacking fault inside the SiC grain. Earlier out-of-pile research work and simulation studies revealed that bulk diffusion of Ag in SiC is rare and not favored.[29] At this point, it is not clear what would be the cause of the intragranular movement of Ag in these two specific cases because no obvious relation to fuel type (identified in Baseline and Variant 1 fuel types) and irradiation level (11.4 and 17.4% FIMA) could be made.

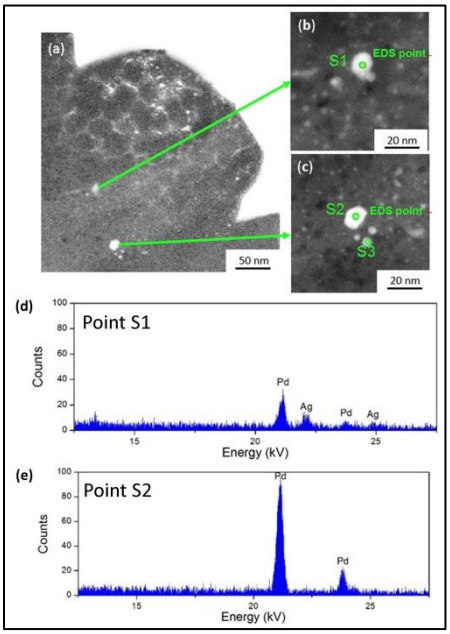

Fig. 5. STEM HAADF images of particle AGR1-632-035 showing (a) a nanometer-sized Pd-Ag precipitates (about 10 to 20-nm diameter) inside the SiC grains at the SiC-IPyC interface and (b) a nanometer-sized Pd precipitate approximately 4 μm inside the SiC layer.[30]

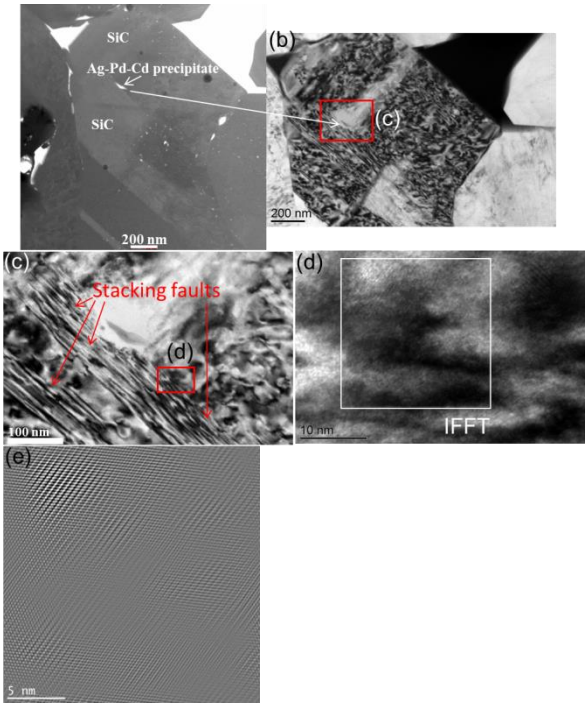

Fig. 6. An Ag-Pd-Cd precipitate at a stacking fault inside a SiC grain of particle AGR1-523-SP01. (a) STEM dark field image showing the location of the Ag-Pd-Cd precipitate, the composition of which was determined by EDS, (b) TEM image corresponding to (a), (c) a magnification of the red rectangle in (b) showing stacking faults with red arrows, (d) a magnification of the red rectangle in (c), where stacking faults are present, (e) inverse Fast Fourier transform (FFT) of the white square in (d), where the continuous lattice fringes indicate absence of grain boundary and confirm the presence of stacking faults.[28]

III.D. Finding of Pd and U both Intergranular and Intragranularly in SiC

Pd was identified both inter- and intra-granularly in the SiC layer from intact TRISO-coated particles. The intragranular Pd-rich precipitates were generally nano-sized and nodular and could also contain small concentrations of Cd and U. These nodules were sometimes observed within the vicinity of planar defects, such as stacking faults or nano twins.[21] Pd-rich precipitates also are present at triple-points and grain boundaries, either alone, or co-existing with Ag and Cd or with U. See Figure 7 for examples of the different types of Pd-containing precipitates observed in particle AGR1-632-035 with Figure 6(a) showing the examination area. The intragranular Pd-rich precipitates are shown in Figure 7(b) labeled as P1 and P2 while Pd-rich triple points are indicated with T1 to T3. Additional precipitates identified in Figure 6(c) are also Pd rich and a honeycomb U-rich network is also shown in Figure 6 (d). The Pd-rich micron-sized precipitates are often found in conjunction with other very low concentration fission products like Sr, Cs, and plutonium (Pu) as well as U (see Refs. 27 and 30, and Figure 7).

It is also important to note that no significant Pd corrosion at the SiC-IPyC interface was observed for all intact AGR-1 particles examined. Only minor interactions were observed during the HRTEM examination of particle AGR1-411-030 (see Ref. 21).

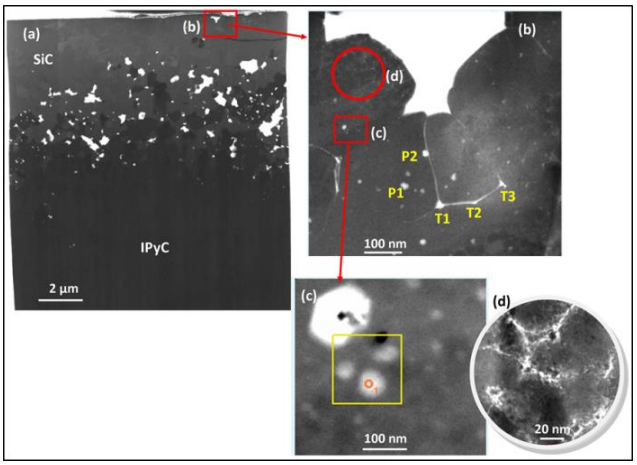

Fig. 7. STEM images of (a) fission-product distribution networks at the SiC-IPyC interlayer of particle AGR1-632-035, (b) higher-magnification image showing intragranular precipitates labeled P1 and P2 as well as the triple points T1-T3 which all contain mainly Pd, (c) higher magnification of the Pd-rich nodules and (d) a honeycomb network of mainly U (adapted from Ref. 30).

III.E. Finding of Cs in SiC

Cs was found in precipitates from the SiC layer of intact TRISO-coated particles in concentrations below 1 at.%. Figure 8 provides examples of micron-and nano-sized precipitates, which contains Cs amongst other elements, for particles AGR1-632-035 (a baseline fuel type) and AGR1-433-001 (Variant 3 fuel type). The micron-sized precipitate in Figure 8(a) consists of Pd-Ag-Cs-U, while the nano-sized precipitates located in triple points contain Pd-Ag-Cs-Eu-U (labeled 2) and Pd-Cs-Pu (labeled 7) respectively as shown in Figure 8(b).

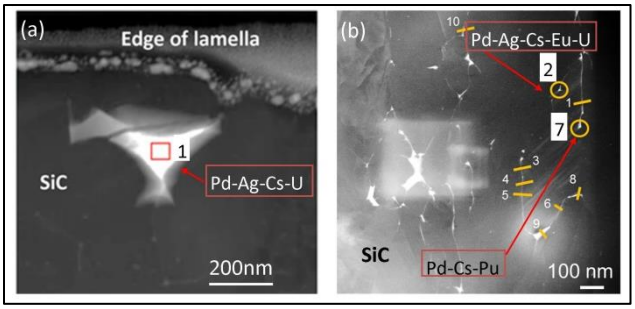

Fig. 8. STEM images of (a) micron size fission-product precipitate located at the SiC-IPyC interlayer of particle AGR1-632-035 found to contain Pd-Ag-Cs-U, (b) precipitates located at triple points in the SiC layer from particle AGR1-433-001 contain Pd-Ag-Cs-Eu-U (labeled 2) and Pd-Cs-Pu (labeled 7) respectively (adapted from Refs. 13 and 30).

III.F. Qualitative Chemical Composition of Fission Product Precipitates Using EDS

Qualitative chemical compositions were measured using EDS in more than 700 precipitates covering multiple areas of each particle from the different compacts.[13] Generally, classification of areas and of corresponding precipitates were made in three regions of the SiC layer called inner, center, and outer areas. The inner area closest to the SiC-IPyC interlayer and the outer area the furthest from the SiC-IPyC interlayer. This was to identify potential changes in chemical element distribution patterns and the combinations of elements from the inside SiC edge to the outside SiC edge.

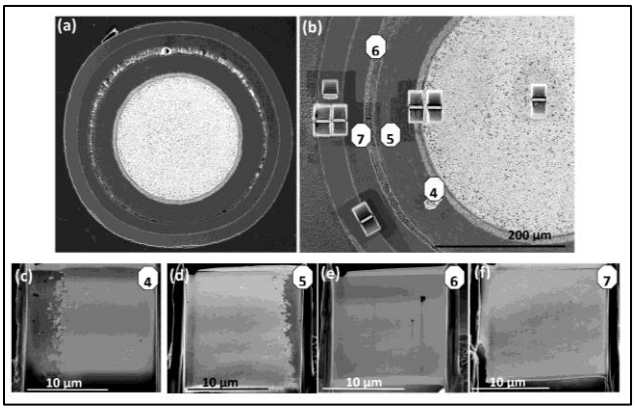

Fig. 9. Images from particle AGR1-433-004 showing the (a) cross section of the particle, (b) actual FIB lamellae locations in the SiC layer labeled 4 through 7, and (c) through (f) actual Lamellae 4 to 7, respectively, used for STEM and EDS examination.

Figure 9 shows an example of the location of these areas for particle AGR1-433-004. Figure 9(a-f) shows the cross section of the particle, the focus ion beam (FIB) preparation location plan, lamellae positions marked, and finally the fabricated lamellae. For this particle, lamellae 4 and 5, which are the closest to the SiC-IPyC layer, represents the inner area while lamellae 6 and 7 represent the center and outer areas respectively.

Figure 10 and corresponding Table V, provide an example of the detailed results performed on each particle from the 20 precipitates analyzed in this area from particle AGR1-433-004 from lamella 4. Predominantly Pd-U precipitates were found with two Pd-U-Sr, one Pd-Sr and one Pd precipitate while no Ag, Cs, cerium (Ce), or Eu were found.

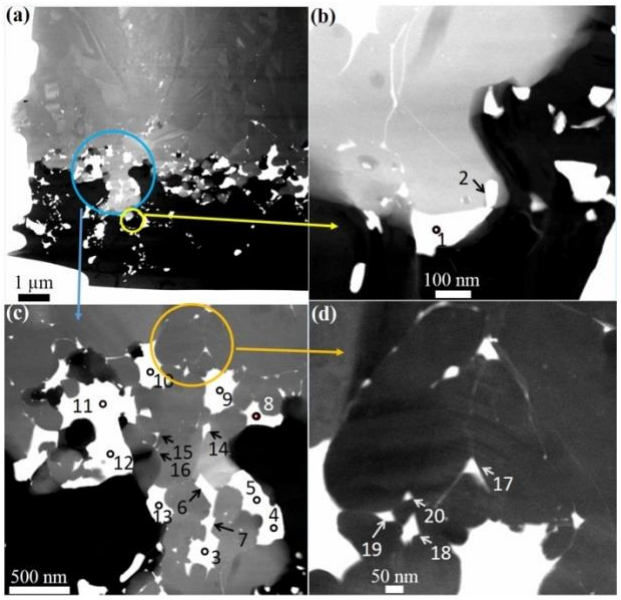

Fig. 10. STEM dark field images of (a) fission product precipitates located at the SiC-IPyC interface of particle AGR1-433-004 (lamella 4), where images (b), (c), and (d) contain larger-magnification images of precipitates numbered 1 through 20.

Table VI presents a summary of all element combinations found in the three SiC regions of the particles examined. The combinations of elements in each precipitate were measured (similar to the example shown in Figure 10 and result reported in Table V). After all the various element combinations present in precipitates for a specific sub-area were listed, the element combinations are then summarized again for the inner, center, and outer areas. Microstructural examination of TRISO-coated particles from several compacts showed micro- and nano-precipitates throughout the SiC layer.

The element combinations reported in Table VI, do not provide information on the effect that precipitate size and location (e.g., grain boundary or triple point, inter- or intra-granular precipitate) have with regards to the different element combination per area.

The various element combinations are found to be complex and varying of nature. Often other elements (e.g., Eu, Ce, Pu, and Cs) can be present in precipitates that predominantly contain Pd, Ag, and U. This complicates the interpretation for determining possible trends with fuel type, level of Ag retention within the particle, and SiC layer location. Additionally, it has not yet been established if the size and location (e.g., present at grain boundary or triple point, inter- or intra-granular precipitates), fuel type, Ag retention, or other unknown factors play a role in the combination of elements. It is observed that Pd is usually present in most of the examined fission products precipitates and was often found separately and throughout the SiC layer. More elements and different element combinations are identified for the safety-tested particles (Compact 4-3-3) compared to the particles only exposed to irradiation (Compacts 6-3-2, 5-3-1, 1-3-1). Additionally, it is observed that the low Ag retention particle (AGR1-433-001) exhibits the most element combinations and contains up to six different elements in a single precipitate. Ce was found in all particles examined; however, it is seldom found separately and mostly in combination with Pd. Eu is not found in the high Ag retention particle AGR-531-031 (Variant 1 fuel) nor in both particles from Compact 1-3-1 (Variant 3). Generally, more element and element combinations exist for precipitates from low-Ag-retention particles compared to the high-retention particles irrespective of fuel type. These observations suggest that the low retention particle's microstructure favorably allow more abundant element combinations. Historically, Cs was not found in intact SiC layers using SEM EDS analysis; however, this study shows the presence of Cs in particles from all compacts evaluated. As UO_2 kernelled fuel were not analyzed using the same advanced techniques, it cannot be concluded that the UCO kernelled AGR-1 fuel is unique in having the Cs in the SiC layers. This may be a topic for future work. Cd is often found in conjunction with Ag and, for the Variant 3 fuel type, Cd is detected up to the center of the SiC layer.[27]

TABLE V. Corresponding qualitative chemical composition (at.%) of the precipitates labeled in Figure 10 from an area at the SiC-IPyC interlayer from particle AGR1-433-004-(lamella 4) (elements are considered to be present with concentrations above 0.2 at.%).

Precipitate No.	Concentration (at.%)								Precipitate Identification
	C	O	Si	U	Pd	Ce	Ag	Sr	
Point scan 1	55.13	0.10	34.17	3.10	7.40	0.03	0	0.04	Pd-U
Point scan 2	76.66	0.07	19.38	0	3.87	0	0	0	Pd
Point scan 3	43.64	0	41.94	9.95	4.35	0	0	0.10	Pd-U
Point scan 4	87.72	0	2.64	2.60	6.97	0.03	0	0.01	Pd-U
Point scan 5	60.63	0	29.38	2.82	6.99	0.07	0	0.07	Pd-U
Point scan 6	44.50	0.02	49.52	1.66	4.22	0	0	0.04	Pd-U
Point scan 7	39.12	0	53.72	2.47	4.59	0	0.03	0.05	Pd-U
Point scan 8	61.96	0	33.08	2.84	2.08	0.02	0	0	Pd-U
Point scan 9	42.37	0	35.80	6.65	14.98	0.11	0	0.06	Pd-U
Point scan 10	42.93	0.08	18.09	6.64	21.48	0.17	0	0.54	Pd-U-Sr
Point scan 11	48.52	0	36.01	3.81	9.27	0	0	2.36	Pd-U-Sr
Point scan 12	52.01	0.20	27.67	6.10	13.93	0.05	0	0	Pd-U
Point scan 13	46.44	0	36.83	5.60	11.06	0.06	0	0	Pd-U
Point scan 14	51.95	0.05	41.41	2.42	4.06	0.06	0	0.02	Pd-U
Point scan 15	53.39	0	39.30	0.98	6.15	0	0	0.16	Pd-U
Point scan 16	61.78	0	36.45	0.38	1.35	0	0	0.02	Pd-U
Point scan 17	50.89	0.07	46.26	0.89	1.72	0.05	0	0.08	Pd-U
Point scan 18	60.30	0	39.02	0.17	0.43	0	0	0.06	Pd-U
Point scan 19	49.36	0.24	40.68	0	9.10	0	0	0.60	Pd-Sr
Point scan 20	59.57	0	39.21	0.52	0.58	0.02	0	0.08	Pd-U

Table VI. Precipitate element combination summary (a detection limit of 0.2 at.% was used to determine if an element was present as measured by STEM EDS analysis). For each particle, results are grouped by the specific area of the SiC layer (inner, center, or outer layer) and by the number of elements observed in the precipitates (one element, two elements, and three or more elements).[13]

Particle	Precipitate Element Combinations in the SiC Layer		
	Inner Area	**Center Area**	**Outer Area**
AGR1-632-035 (High (79%) Ag retention)	Pd, Ag	Pd, Ag, Ce	Pd
	Pd-Ag, Pd-Pu, Pd-U, Pd-Ce	Pd-Ag, Pd-U, Pd-Ce,	Pd-Ag, Pd-Eu, Pd-Ce
	Pd-Ag-Cd, Pd-U-Pu, Pd-Ag-Cs-U		Pd-Ag-Ce, Pd-Ce-Eu
AGR1-531 - 038 (Low (< 19%) Ag retention)	Pd	Pd, Ag	Pd
	Pd-U, Pd-Pu, Pd-Ag	Pd-Ag, Pd-Pu, Pd-U, Pd-Ce	
	Pd-Cs-Eu, Pd-Ce-Eu, Pd-Cs-Ag, Pd-U-Pu, Pd-Ag-Eu	Pd-Ag-U, Pd-U-Pu, Pd-Ag-Pu	Pd-U-Pu
AGR1-531 - 031 (High (105%) Ag retention)	Pd, Cs, Pu, U, Ce,		
	Ag-U, Cs-U, Ce-U, U-Pu		
AGR1-131-066 (High (39%) Ag retention)	Pd, U	Pd	Pd
	Pd-Si, U-Si, Pd-U, Cs-U	Pd-Si, Pd-U	Pd-U, Pd-Ce
	Pd-Si-U	Pd-Si-U	Pd-Ce-U
AGR1-131-099 (Low (<6%) Ag retention)	Pd, U	Pd	Pd
	Pd-U, U-Cs, Pd-U	Pd-U	Pd-U
	Pd-U-Ce, Pd-U-Cs		
	Pd-U-Cs-Ce		
AGR1-433-001 (Low (66%) Ag retention)	Ag, Pd	Pd	Pd
	Ag-Cs, Pd-Ce, Pd-Ag, Pd-U, Ce-U, Pd-Pu	Pd-U,	Pd-Ag, Pd-Eu, Pd-Ce
	Pd-Ag-Ce, Pd-Ce-U, Pd-Ce-Pu, Pd-U-Pu, Pd-Ag-U	Pd-Ce-Eu, Pd-Cs-Pu, Pd-Ce-U	Pd-Eu-U
	Pd-Ce-U-Pu, Pd-Eu-U-Pu, Pd-Ce-Eu-U, Pd-U-Pu-Ce	Pd-Ce-Eu-Pu, Pd-Ag-Ce-Eu	Pd-Ag-Cs-Eu-U
		Pd-Ag-Cs-Eu-U	
		Pd-Ag-Ce-Eu-U-Pu	
AGR1-433-004 (High (98%) Ag retention)	Pd, Ag	Pd	Pd
	Pd-U, Pd-Ce, Pd-Ag, Pd-Eu	Pd-Ce	Pd-Ag
	Pd-Ce-Pu, Pd-U-Pu, Pd-Ag-Ce		Pd-Cs-Eu

III.G Quantitative Chemical Composition of Fission Product Precipitates Using APT

Development work on APT is a collaborative effort with the University of Wisconsin-Madison and Boise State University. Due to the brittle nature of irradiated SiC, initial work on quantitative chemical composition analysis using APT was limited, achieving only a small analytical depth in the FIB-prepared APT tips during the analysis.

However, during December 2015, the first successful APT results on neutron-irradiated SiC were achieved from particle AGR1-632-034 (see Ref. 31). To reach this point, many lessons were learned and addressed.

During the first few APT runs, useful data were not obtained due to frequent tip fractures. Contributing towards these fractures were the presence of a surface oxidization layer of about two nanometers thickness, flexible copper grids, inherent properties of irradiated SiC, formation of an amorphous surface layer during FIB

sample preparation, and the inconsistent profile contours of the tips. In addition, one of the biggest challenges was to prepare tips with the fission product features in the top center of the tip to a depth of <100 nm from the tip point. This required a highly skilled FIB operator as many of the precipitates were not visible at the SEM resolution. Additionally, the distance between the FIB and APT facilities contributed to oxidation of the tips. This was partially resolved later by modification to the packaging method and transport logistics.

One of the largest challenges was to obtain a large enough volume of SiC to encounter features of interest due to the extremely brittle irradiated SiC sample, which has low electric and thermal conductivities, as well as big differences in the evaporation field needed in local electron atom probe (LEAP) runs between C (142 V/nm C+, 103 V/nm C++) and Si (45 V/nm Si+ and 33 V/nm Si++). By tailoring LEAP running parameters, the mode, sample-setting temperature, laser energy, and pulse frequency for optimized SiC APT, data were obtained for unirradiated surrogate and irradiated TRISO samples. The most effective LEAP parameters which were applied to obtain the data in this paper are shown in Table VII.

Table VII. The most effective LEAP parameters determine to date (adapted from Ref. 31).

	Unirradiated SiC	**Neutron Irradiated SiC**
Specimen temperature (K)	90	95
Laser pulse energy (pJ)	100	300
Pulse frequency (kHz)	200	125

Representative scanning TEM HAADF images of an atom probe sample tip from unirradiated surrogate TRISO fuel and corresponding reconstructed 3D elemental maps of C and Si are shown in Figure 11. The diameter of the sample tip apex is about 50 nm. C and Si atoms are uniformly distributed in the volume (48 × 49 × 293 nm). Quantitative analysis shows that concentrations of C and Si within this volume are 44.81 at.% (error 0.01 at.%) and 53.96 at.% (error 0.01 at.%), respectively. About 1.2 at.% O was also detected within this volume, which could be mostly attributed to the air. More APT data were also obtained from the unirradiated surrogate TRISO fuel samples and they show similar concentrations of C and Si of about 45 at.% and 54 at.%, respectively. This may indicate non-stoichiometry of the SiC and the results needs to be explored in more depth.

Figure 12 shows a STEM image of an irradiated TRISO APT tip (Figure 12[a]) and corresponding LEAP data (Figure 12[b] and [c]). An Ag-Pd-U phase is identified at one side of the reconstructed volume (Figure 12[b]) which corresponds to the circled region in Figure 12(a). The mass spectrum (Figure 12[c]) clearly indicates an isotope of ^{109}Ag+ among Pd isotopes, as well as ^{235}U+2 and ^{238}U+2 isotopes. By selecting 3 at.% Pd as an interface, a proxigram calculated across the interface (Figure 13) clearly indicates a Pd-, Ag-, and U-enriched phase. This phase also contains Si and some C (note only the fission products Ag, Pd and U are shown). A 3-D elemental map of a smaller volume (6 × 6 × 6 nm^3), selected to exemplify this Pd-Ag-U-rich phase, is shown in Figure 14.

Quantitative analysis within the Pd-Ag-U-rich phase shows the normalized concentrations of Pd, Ag, U, Si, and C are 12.1 at.% (error 0.3 at.%), 3.5 at.% (error 0.2 at.%), 3.3 at.% (error 0.1 at.%), 60.0 at.% (error 0.3 at.%), and 21.2 at.% (error 0.2 at.%), respectively.

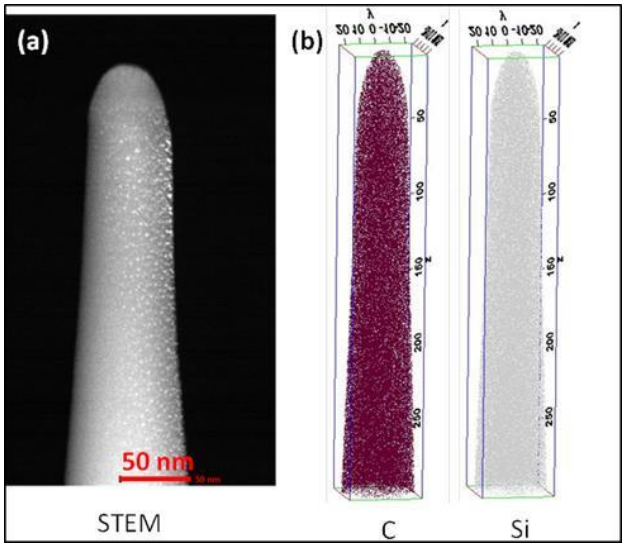

Fig. 11. STEM HAADF image of an unirradiated surrogate TRISO APT sample tip (a) and corresponding reconstructed three-dimensional APT maps of C and Si in a volume size of 48 × 49 × 293 nm (b). [31]

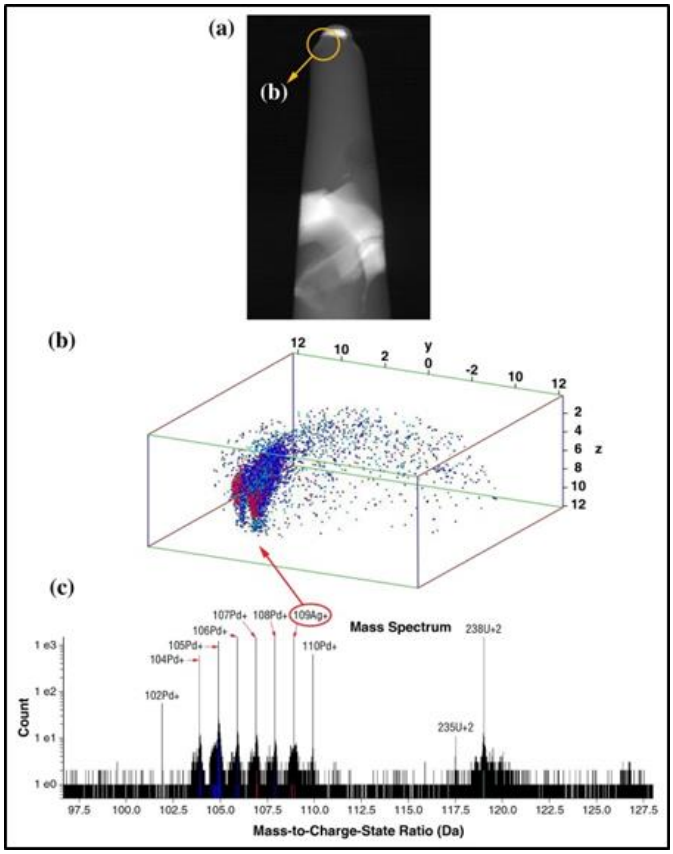

Fig. 12. STEM HAADF image of an irradiated TRISO APT sample tip (a), corresponding reconstructed three-dimensional APT maps showing an Ag-Pd-U-rich phase in a volume size of 32 × 31 × 12 nm^3 (Ag labeled red), Pd labeled blue and U labeled turquoise) (b) and mass spectrum showing detected isotopes of Ag, Pd and U (c).[31]

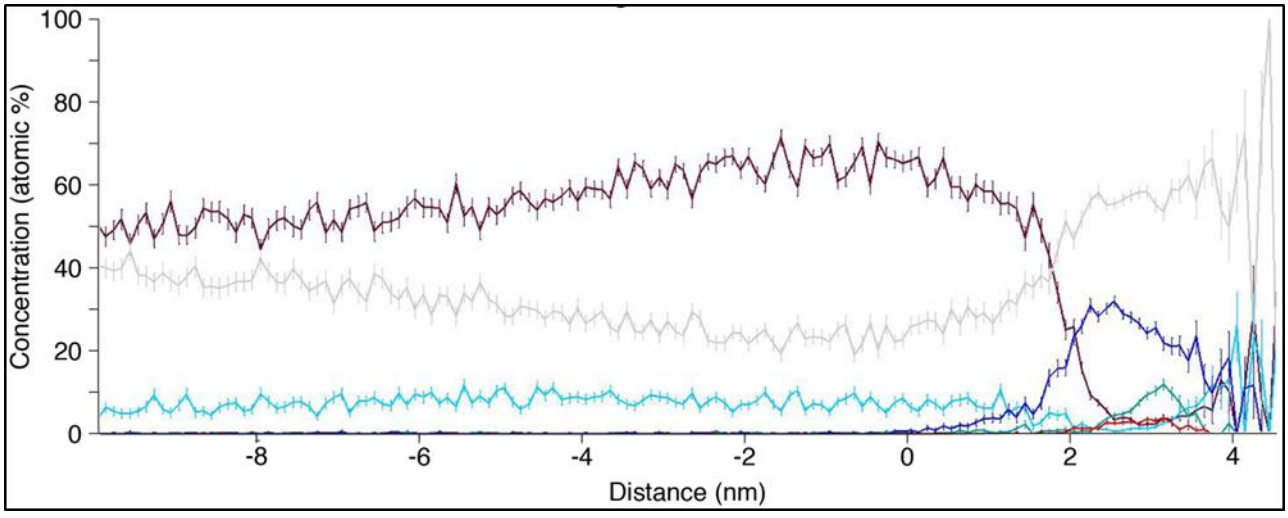

Fig. 13. Proxigram with respect to a 3 at.% Pd iso-concentration surface, clearly indicating a Pd (blue), Ag (red), and U (turquois) enriched phase. This phase also contains Si (grey) and some C (brown) (note only the fission products Ag, Pd and U are shown).[31]

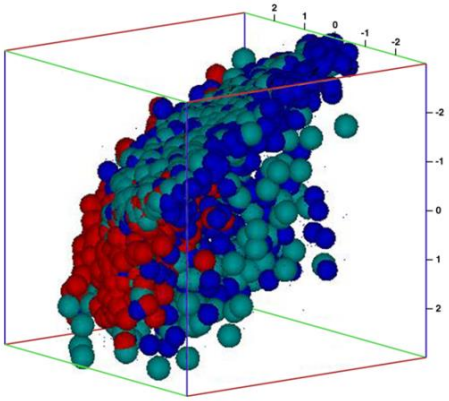

Fig. 14. 3-D elemental map of Pd (blue), Ag (red), and U (turquois) in a selected small volume of 6 × 6 × 6 nm^3 (see Ref. 31).

III.H. Structure of Fission-product Precipitates

To date, limited information is available on the structure and phases of the precipitate due to the complex nature and large variety of precipitates that exist.

HRTEM investigations were recently undertaken on particles from Variant 3 fuel type particles (Compact 1-3-1 and Compact 4-3-3). Multi- and single-phase precipitates were identified in both the IPyC layer of particle AGR1-131-099, lamella 1 and 5 (see Figure 15), as well as in the SiC layer (Figure 16), based on the elemental composition. Crystallographic examination also confirmed this finding. The interface between SiC and a fission-product precipitate was well-defined and free of porosity (see Figure 17). From the change in tilt of the atomic layers across this interface, it appears that the secondary phase is not aligned to the SiC in any well-defined manner.[19]

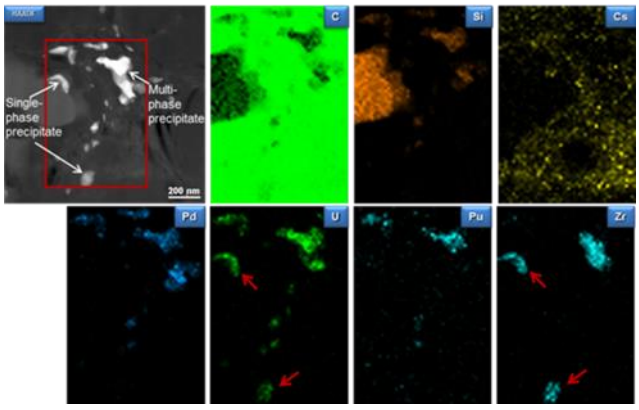

Fig. 15. STEM image and EDS mapping of a small area containing precipitates in the IPyC layer of particle AGR1-131-099 close to the IPyC-SiC interface. Both single- and multi-phase precipitates are shown. The red arrows indicate the single phase precipitate.[19]

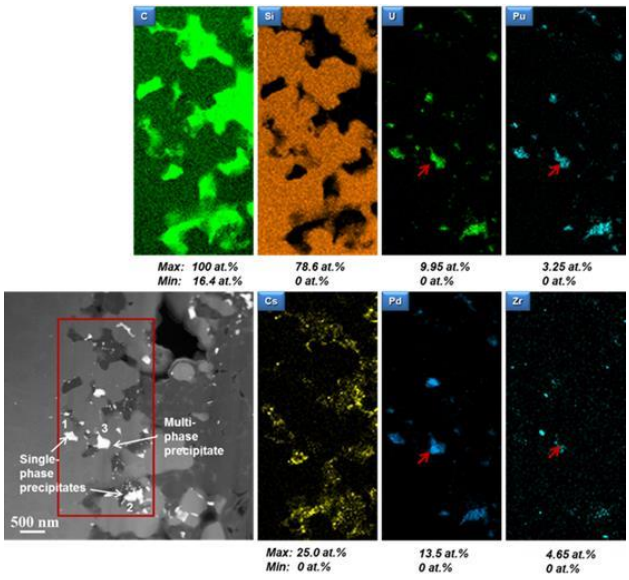

Fig. 16. STEM image and EDS mapping of an area containing precipitates in the SiC layer of particle AGR1-131-099 close to the IPyC-SiC interface. Both single- and multi-phase precipitates are shown. The red arrows indicate the multi-phase precipitate.[19]

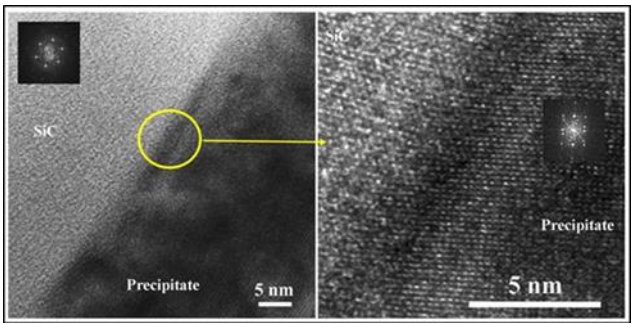

Fig. 17. HRTEM images of the interface between a fission-product precipitate and the SiC matrix in particle AGR1-131-099 lamella 1 (see Ref. 19).

High-resolution STEM examination was performed on particle AGR1-433-001 in the inner area (lamella 05) of the SiC layer approximately 5 µm from the SiC-IPyC interface. Simultaneous bright and atomic (Z) contrast dark-field STEM imaging of a Pd-rich fission product precipitates in the SiC layer are shown in Figure 18(a) and (b), respectively. A single Pd-rich fission product precipitate at a triple junction in the SiC (Figure 18[c]), outlined by the white box, was imaged using atomic-resolution transmission electron microscopy. Figure 18(d) shows the lattice resolution image of the precipitate marked in (Figure 18[c]). This feature was explicitly studied in detail, and in Figure 18(e) the same (Figure 18[d]) 100 cubic fission product precipitate was found to be bordering on a 101 SiC lattice (Figure 18[g]). Note the accompanying modeled

lattices for the cubic fission product precipitate and SiC are also provided for each of these features. The qualitative composition at the fission product precipitates (shown in Figure 18[c]), based on point-resolved EDS, was: C 35.4%, O 15.3%, Si 44.1%, Pd 3.8%, and Eu 0.5%. Values are reported in relative atomic percentages based on standardless quantification with an estimated uncertainty of 0.2 at.%.

Atomic contrast STEM (Figure 19 [a]) and atomic resolution aberration-corrected TEM (Figure 19[b]) were performed to resolve fission product precipitates, including a Pd-Ag precipitate outlined by a white circle, trapped at a triple junction within the intact SiC coating from particle AGR1-433-001. EDS confirms the intact precipitate chemistry as 3.8 at.% Pd, and 0.8 at.% Ag (Figure 19[c]).

The single Pd-Ag fission product precipitate, at a triple junction in the SiC was imaged using atomic-resolution transmission electron microscopy at various levels of magnification to include the resolution to resolve the crystal structure of the sample. Based on the atomic resolution images collected inside an aberration-corrected FEI Titan transmission electron microscope operated at 300 kV with 0.8 Angstrom point-point resolution, a cubic structure of the precipitate was determined based on selected area fast-Fourier transforms (FFTs) of the multiple images (Figure 19 [d]). Similar trace FFTs (Figure 19 [e-g]) of the surrounding SiC domains A, B, and C noted in Figure 19 (a) resolve the cubic structure of SiC. EDS values are reported in relative atomic percentages, based on standardless quantification with an estimated uncertainty of 0.2 at.%).

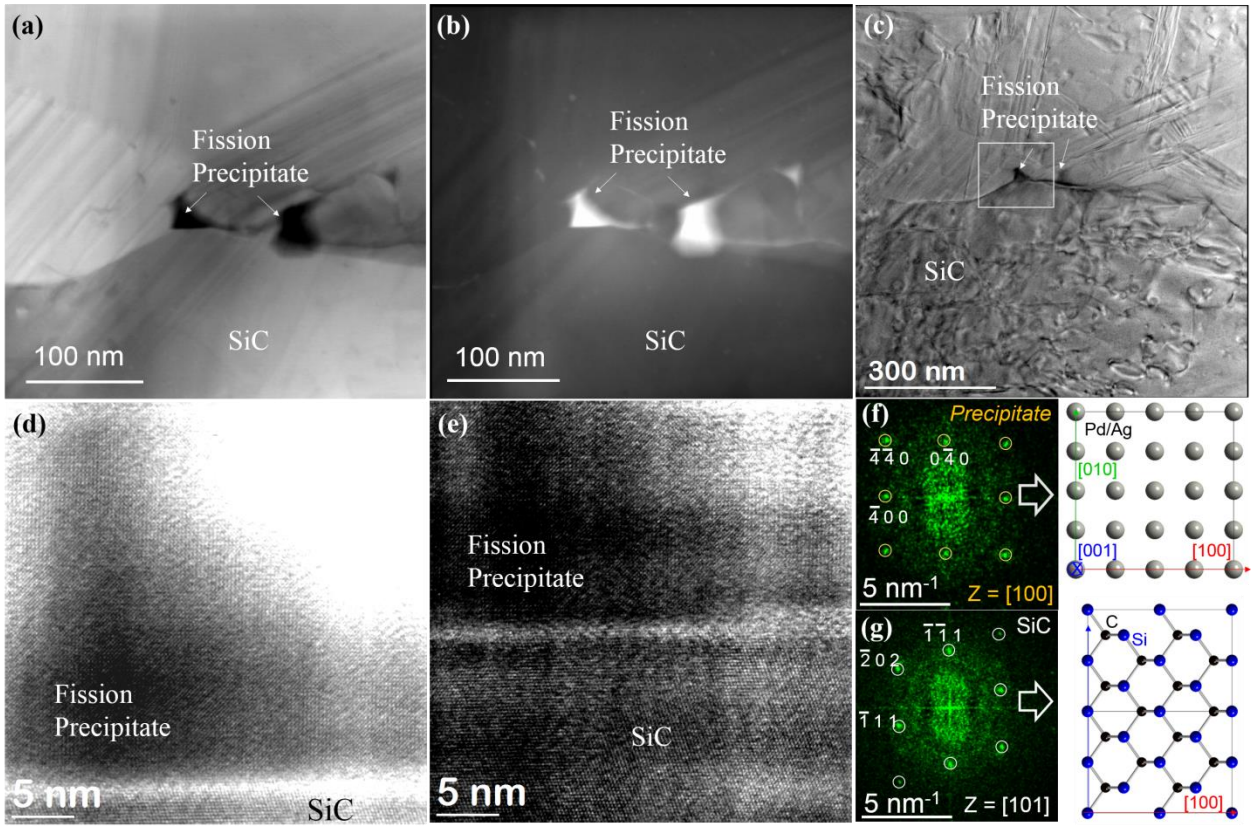

Fig. 18. STEM examination in the inner area (lamella 05) of the SiC layer approximate 5 µm from the SiC-IPyC interface of particle AGR1-433-001 shows simultaneous (a) bright- and (b) atomic contrast dark-field STEM images of fission product precipitates contained within the SiC layer, (c) A single Pd-rich fission product precipitate at a triple junction in the SiC, outlined by the white box, was subsequently imaged using atomic-resolution Cs corrected transmission electron microscopy. The accompanying (d) lattice resolution image of the precipitate marked in (c) was explicitly studied in detail, where in (e) the same (f) 100 cubic fission product precipitate was found to be bordering on a (g) 101 SiC lattice. Note the accompanying modeled lattices for the cubic fission product precipitate and SiC are also provided for each of these features.

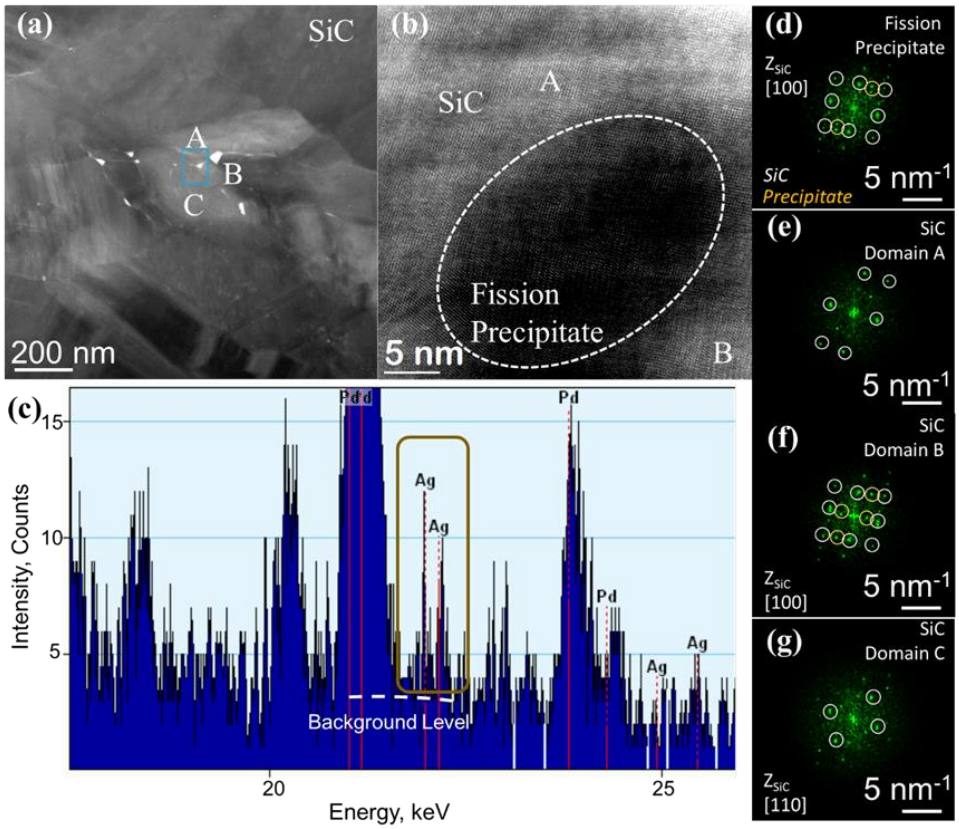

Fig. 19. (a) Dark field STEM, (b) Cs-corrected TEM images of a Pd-Ag precipitate outlined by a white circle, (c) EDS confirms the intact precipitate chemistry as 3.8 at.% Pd, and 0.8 at.% Ag (reported as relative composition); the single Pd-Ag fission product precipitate, at a triple junction in the SiC, was imaged using atomic-resolution transmission electron microscopy at 1Mx magnification, (d) the cubic structure of the precipitate was resolved based on selected area fast-Fourier transforms (FFTs) of the multiple images, (e–g) similar trace FFTs of the surrounding SiC domains A, B, and C noted in (a) resolve the structure of SiC. Note the diffraction spots corresponding to the precipitate and SiC are circled in orange and white respectively for trace FFTS (d-g). Furthermore for the SiC lattice where all points indexed represent a specific zone axis that orientation is provided in white text.

III.I. Techniques to Determine Crystallographic Information (EBSD, TKD, PED)

To determine the influence of grain-boundary character on fission-product migration in SiC, it was necessary to employ techniques that can determine the misorientation across individual grain boundaries, including grain boundaries that contain fission products, as well as those that do not contain fission products. While SEM-based electron backscattered diffusion (EBSD) can determine grain-boundary misorientation, it is not possible to identify nano-sized fission-product precipitates on the grain boundaries or identify the composition of these precipitates.

Transmission Kikuchi diffraction (TKD) or t-EBSD, a method similar to conventional EBSD, was also considered and although an order-of-magnitude improvement in spatial resolution was achieved compared with EBSD, it still did not provide significant resolution to provide crystallographic information at areas of 2–5 nm. Precession electron diffraction (PED) was explored as the advantage of PED is that it uses a very small electron-beam spot size (≈5 nm or less) and the interaction volume is on the order of the beam size because the sample is very thin. Both enable a very small step size and high spatial resolution, allowing orientation analysis at the nano-level. Recently, successful correlations with fission-product transport and grain-boundary characteristics were achieved using PED and will be reported separately at this conference in another paper, namely HTR 2016 paper 18560 (see Ref. 14).

IV. DISCUSSION AND CONCLUSIONS

The AGR-1 post-irradiation advanced microscopy and micro-analytical examination provided substantive new information on fission-product behavior and microstructural changes due to irradiation. The deployment and adaption of advanced nano-scaled techniques set a benchmark for future studies.

Most significant is the finding that Ag is identified at both intra- and inter-granular sites within the SiC microstructure, although it is predominantly in grain boundaries and triple points. It was further found that Pd dominated most of the fission product precipitates examined and is often found throughout the SiC layer thickness, either separately or co-existing, with other elements. Qualitatively, the general Pd composition is greater than the Ag content, although no specific trend was further found relating the Pd to Ag ratios of the precipitates to the location in SiC. This is consistent with the relative amount of Pd and Ag generated during fission (the total Pd inventory is much higher than Ag).

In addition, the combinations of elements in more than 700 precipitates that were examined, from a variety of different particles, are complex and varying in nature and often other elements (e.g., Eu, Ce, Pu, and Cs) can be present in precipitates that predominantly contain Pd, Si, Ag, and U. This complicates the interpretation for determining possible trends with fuel type, level of Ag retention within the particle, and SiC layer location. Generally, more element combinations exist for precipitates from particles with relatively low Ag retention compared to particles with relatively high Ag-retention irrespective of fuel type. U is predominantly found in combination with other elements and is only found alone in precipitates from Compact 1-3-1, which is a Variant 3 fuel compact. U and Ag are only found as a combination in the low Ag retention safety-tested particle AGR1-433-001. Historically, Cs was not found in intact SiC layers; however, this study shows the presence of Cs in particles from all compacts evaluated.

Although this work was not predominantly focused on fission product mechanistic studies, most of the results and observations contributed toward knowledge on transport mechanisms. From this work, no single mechanism hypothesis can be reported. The complexity of mechanisms is further highlighted by the multiple variations of elemental combinations found in the fission product precipitates. This may indicate that various transport mechanisms are present, depending on specific irradiation conditions. In addition, it seems that movement of Ag is not assisted by a specific element in all cases due to the fact that various element combinations were identified and Ag was also found separately from any other fission products or U. Therefore, it is not necessarily true that a chemical-assisted transport mechanism is dominant. The presence of Ag predominantly on grain boundaries suggests that grain boundary transport mechanism may be prominent.

Neutron damage and its effects on fission-product transport were not examined during PIE activities due to prioritization on fission product distribution, chemical composition, and grain-boundary characteristics. However, this is a very important microstructural effect that needs to be considered in transport mechanistic studies. The alignment of voids on grain boundaries in the vicinity of Pd-containing precipitates, within the SiC grains and at the triple point precipitates on actual irradiated AGR-1 TRISO coated particle AGR1-632-035, shows a potential effect on transport mechanisms. This is further demonstrated with recent out-of-pile research that has been conducted [32, 33] Earlier AGR-1 microscopy examination also showed that voids, due to irradiation damage, are aligned on grain boundaries in the vicinity of the precipitates.[8,23] Other research also showed that Ag transport is enhanced by neutron irradiation.[32,33] It is hypothesized that the Ag-transport mechanism is likely more complex and may be a combination of several mechanisms.[26] It is recommended that further work is performed on irradiated TRISO particles from the AGR-1 and AGR-2 experiments on this topic.

Additionally, more lamellae per particle need to be examined as preliminary PED and STEM studies showed potential preferential fission product transport, which may skew trend analysis comparing particle to particle. Although APT provided successfully atomic distribution and composition of the precipitate, it is not fully implemented due to the low success rate in producing precipitate-containing tips for analysis. It is also further recommended that structural identification of the precipitates using HRTEM to continue.

In conclusion, the evidence provided in this report and associated references showed significant new results describing not only the behavior of TRISO fuel particles during irradiation testing, but also information contributing toward understanding of fission transport mechanisms.

ACKNOWLEDGMENTS

This work was sponsored by the U.S. Department of Energy's Office of Nuclear Energy, under U.S. Department of Energy Idaho Operations Office Contract DE-AC07-05ID14517, as part of the Advanced Reactor Technology Program and the Nuclear Scientific Users Facility–Rapid Turnaround Experiments program. We would like to express our gratitude towards the following researchers: Scott Ploger & Jason Harp (mount and decontamination preparation for electron microscopy examination and micro-analysis), Jim Madden (FIB-STEM and APT sample preparation), Tammy Trowbridge (SEM images used in montages), John Hunn & Tyler Gerczak (IPyC breached-particle collaboration), Bin Leng (STEM and APT [NSUF]), Joanna Taylor and Kristi McIntire (CAES laboratory management), Jhonathan Rosales (combination

of elements tabulation), and Jan Neethling and Jaco Oliver (HRTEM). We thank Dr. Paul Demkowicz of Idaho National Laboratory for providing data concerning experiment setup and execution.

REFERENCES

1. D. A. PETTI, J. T. MAKI, J. D. HUNN, P. J. PAPPANO, C. M. BARNES, J. J. SAURWEIN, S. NAGLEY, J. KENDALL, and R. HOBBINS, "The DOE Advanced Gas Reactor Fuel Development and Qualification Program," *JOM*, **62**, 62 (2010).
2. DAVID PETTI, "Project Execution Plan for the VHTR Technology Development Office," Idaho National Laboratory, PLN-2494, Revision 0, (2008).
3. R. B. MORRIS, C. A. BALDWIN, P. A. DEMKOWICZ, J. D. HUNN, and E. L. REBER, "Performance of AGR-1 High-Temperature Reactor Fuel During Post-Irradiation Heating Tests," *Nuclear Engineering and Design 306 (2016) 24-35 Nucl. Eng. Des.*, **306**, 24 (2016).
4. J. D. HUNN, G. E. JELLISON, JR., and R. A. LOWDEN, "Increase in Pyrolytic Carbon Optical Anisotropy and Density During Processing of Coated Particle Fuel Due to Heat Treatment," *J. Nucl. Mater.*, **374**, 445 (2008).
5. B. P. COLLINS, "AGR-1 Irradiation Test Final As-Run Report," Idaho National Laboratory, INL/EXT-10-18097, Rev. 1 (2012).
6. M. BARRACHIN, R. DUBOURG, M. P. KISSANE, and V. OZRIN, "Progress in Understanding Fission-Product Behaviour in Coated Uranium-Dioxide Fuel Particles," *J. Nucl. Mater.*, **385**, 372 (2009).
7. M. BARRACHIN, R. DUBOURG, S. DE GROOT, M. P. KISSANE, and K. BAKKER, "Fission-Product Behaviour in Irradiated TRISO-Coated Particles: Results of the HFR-Eu1bis Experiment and their Interpretation," *J. of Nucl. Mater.*, **415**, 104 (2011).
8. I. J. VAN ROOYEN, B. D. MILLER, D. E. JANNEY, J. RIESTERER, P. A. DEMKOWICZ, and J. HARP, "Electron Microscopic Examination of Irradiated TRISO Coated Particles of Compact 6-3-2 of AGR-1 Experiment," Idaho National Laboratory INL/EXT-11-23911 (2012).
9. B. G. KIM, S. J. PARK, S. T. HONG, B. C. LEE, K-C JEONG, Y-K KIM, W. K. KIM, Y. W. LEE, M. S. CHO, and Y. W. KIM, "Irradiation Device for Irradiation Testing of Coated Particle Fuel at Hanaro," *Nucl. Eng. Tech.,* **45**, *7,* 941 (2013).
10. I. J. VAN ROOYEN, Y. Q. WU, T. M. LILLO, T. L. TROWBRIDGE, J. M. MADDEN, and D. GORAN, "Advanced Electron Microscopic Techniques Applied to the Characterization of Irradiation Effects and Fission Product Identification of Irradiated TRISO Coated Particles from the Agr-1 Experiment," *Global 2013 Conference Proceedings*, Salt Lake City, September 29, 2013.
11. H. CURTIUS et al., "Spent UO2 TRISO Coated Particles – Instant Release Fraction and Microstructure Evolution," *Radiochim. Acta*, **103** *6*, 433 (2015).
12. J. D. HUNN, T. J. GERCZAK, R. N. MORRIS, C. A. BALDWIN, and F. C. MONTGOMERY, "PIE on Safety-Tested Loose Particles from AGR-1 Compact 4-4-2," ORNL/TM-2015/161, (April 2016).
13. I. J. VAN ROOYEN, T. LILLO, H. WEN, K. E. WRIGHT, J. MADDEN, and J. AGUIAR, "Advanced Electron Microscopy and Micro Analytical Technique Development and Application on Irradiated TRISO-Coated Particles from the AGR-1 Experiment," Idaho National Laboratory, INL/EXT-15-36281 (in preparation 2016).
14. T. M. LILLO, I. J. VAN ROOYEN, and J. A. AGUIAR, "Silicon Carbide Grain Boundary Distributions, Irradiation Conditions, and Silver Retention in Irradiated AGR-1 TRISO Fuel Particles," HTR2016, Las Vegas, Nevada, 7–10, paper 18560, (November 2016).
15. K. E. WRIGHT and I. J. VAN ROOYEN, "Electron Probe Micro-analysis of Irradiated and 1600°C Safety-Tested AGR-1 TRISO Fuel Particles with Low and High Retained 110mag," HTR2016, Las Vegas, Nevada, 7–10, paper 18570, (November 2016).
16. P. A. DEMKOWICZ, J. M. HARP, P. L. WINSTON, and S. A. PLOGER, "Analysis of Fission Products on the AGR-1 Capsule Components," Idaho National Laboratory, INL/EXT-13-28483, Rev. 0 (2013).
17. J. M. HARP, "Analysis of Individual Compact Fission Product Inventory and Burnup for the AGR-1 TRISO Experiment Using Gamma Spectrometry," Idaho National Laboratory, ECAR-1682, Revision 3 (2014).
18. J. D. HUNN, C. A. BALDWIN, T .J. GERCZAK, F. C. MONTGOMERY, R. N. MORRIS, C. M. SILVA, P. A. DEMKOWICZ, J. M. HARP, and S. A. PLOGER, "Detection and Analysis of Particles with Failed SiC in AGR-1 Fuel Compacts," . *Nucl. Eng. Des.*, **306**, 36 (2016).

19. P. A. DEMKOWICZ, J. D. HUNN, R. N. MORRIS, I. VAN ROOYEN, T. GERCZAK, J. M. HARP, and S. A. PLOGER, "AGR-1 Post Irradiation, Examination Final Report," Idaho National Laboratory INL/EXT-15-36407 (2015).
20. P. A. DEMKOWICZ, E. L. REBER, D. M. SCATES, L. SCOTT, "First High Temperature Safety Tests of AGR 1 TRISO Fuel with the Fuel Accident Condition Simulator (FACS) Furnace," *J. Nucl. Mater.*, **464**, 320 (2015).
21. I. J. VAN ROOYEN, E. J. OLIVIER, and J. H NEETHLING, "Investigation of the Fission Products Silver, Palladium and Cadmium in Neutron Irradiated SiC using a Cs Corrected HRTEM," *J. Nucl. Mater.*, **476** 931 (2016).
22. T. M. LILLO and I. J. VAN ROOYEN, "Influence of SiC Grain Boundary Character on Fission Product Transport in Irradiated TRISO Fuel," *J. Nucl. Mater.*, **473**, 83 (2016).
23. I. J. VAN ROOYEN, D. JANNEY, B. MILLER, P. DEMKOWICZ, and J. RIESTERER, "Electron Microscopic Evaluation and Fission Product Identification in Irradiated TRISO Coated Particles from the AGR-1 Experiment: A Preliminary Review," *Nucl. Eng. Des.*, **271**, 114 (2014).
24. I. J. VAN ROOYEN, C. HILL, H. WEN, and T. TROWBRIDGE, "Scanning Electron Microscopic Examination of Irradiated TRISO Coated Particles of Compacts 4-1-1, 5-3-1, 1-3-1 and Safety Tested Compact 4-3-3 of AGR-1 Experiment," Idaho National Laboratory, INL/EXT-15-36278 (in preparation 2016).
25. I. J. VAN ROOYEN, Y. Q. WU, and T. M. LILLO, "Identification of Silver and Palladium in Irradiated TRISO Coated Particles of the AGR1 Experiment," *J. Nucl. Mater.*, **446**, 178 (2014).
26. I. J. VAN ROOYEN, H. NABIELEK, J. H NEETHLING, M. J. KANIA, and D. A. PETTI, "Progress in Solving the Elusive Ag Transport Mechanism in TRISO Coated Particles: 'What's new?'," *Proc. of the HTR2014*, Weiha, China, October 27–31, 2014, HTR2014-3-1261.
27. H. WEN, I. J. VAN ROOYEN, C. HILL, T. TROWBRIDGE, and B. CORYELL, "Fission Product Distribution in TRISO Coated Particles Neutron Irradiated to 3.22 × 1025 n/m^2 Fast Fluence at 1092°C," *ASME Power and Energy 2015*, San Diego, California, June 28–July 2, 2015.
28. H. WEN and I. J. VAN ROOYEN, "Advanced Electron Microscopy Study of Fission Products Pd, Ag and Cs in Carbon Areas in the Locally Corroded SiC Layer in a Neutron Irradiated TRISO Fuel Particle," (article in preparation).
29. H. X. XIAO, Y. ZHANG, L. L. SNEAD, V. SHUTTHANANDAN, H. Z. XUE, and W. J. WEBER, "Near Surface and Bulk Behaviour of Ag in SiC," *J. Nucl. Mater.*, **420**, 123 (2012).
30. B. LENG, I. J. VAN ROOYEN, Y. WU, I. SZLUFARSKA, and K. SRIDHARAN, "STEM/EDS Analysis of Fission Products in Irradiated TRISO Coated Particles of the AGR-1 Experiment", *J. Nucl. Mater.*, **475** 62 (2016).
31. Y. Q. WU, I. J. VAN ROOYEN, J. W. MADDEN, J. BURNS and H. M. WEN, "Atom Probe Tomography Characterization on TRISO fuels," (journal article in preparation).
32. J. H. O'CONNELL, and J. H. NEETHLING, "Ag Transport in High Temperature Neutron Irradiated 3C-SiC," *J. Nucl. Mater.*, **455**, 20 (2014).
33. I. SZLUFARSKA, D. MORGAN, J. BLANCHARD, "Ag Transport Through non-Irradiated and Irradiated SiC, Technical Report," DOE/NEUP-11-2988 (2016).